BMC Medical Imaging

RESEARCH

Open Access

Habitat analysis of iron deposition in the basal ganglia for diagnosing cognitive impairment in chronic kidney disease: evidence from a case-control study

Hao Wang[1†], Yu Qi[2†], Xu Liu[3], Li-Jun Song[1], Wen-Bo Yang[1], Ming-An Li[1], Xiao-Yan Bai[1], Mao-Sheng Xu[4,5], Hao-Nan Zhu[4,5], Si-Qing Cai[6,7], Yi Wang[6], Zheng-Han Yang[1], Yuan-Zhe Li[6,7*], Zhen-Chang Wang[1*] and Yi-Fan Guo[4,5*]

Abstract

Background Chronic kidney disease induces alterations in the heterogeneity of iron deposition within the basal ganglia. Quantitative analysis of the heterogeneity of iron deposition within the basal ganglia may be valuable for diagnosing chronic kidney disease-related cognitive impairment.

Methods In this prospective observational cohort study, quantitative susceptibility mapping (QSM) was performed in chronic kidney disease patients. Susceptibility values of each nucleus within the basal ganglia were measured. Radiomic features were extracted from habitats of the basal ganglia on QSM images. Habitat-based models for diagnosing cognitive impairment were constructed using the random forest algorithm. Logistic regression was employed to build the clinical model and the combined model. The performance of each model was evaluated by the receiver operating characteristic (ROC) analysis.

Results A total of 146 patients (mean age, 51 ± 13 years; 92 male) were included, of which 79 had cognitive impairment. The two habitats-based model achieved an area under the curve of 0.926 (95% CI 0.842-1.000) on the test set, the highest among all prediction models. The two-habitat maps indicated that chronic kidney disease had two distinct patterns of impact on iron deposition in the basal ganglia region. The capability of the two habitats-based model to identify chronic kidney disease-related cognitive impairment was significantly superior to that of the susceptibility values measured in various nuclei (all $p < 0.05$).

Conclusions This study innovatively applied a habitat-based quantitative analysis technique to QSM, successfully constructing a model that accurately diagnoses chronic kidney disease-related cognitive impairment.

†Hao Wang and Yu Qi contributed equally to this work.

*Correspondence:
Yuan-Zhe Li
ctmr@fjmu.edu.cn
Zhen-Chang Wang
cjr.wzhch@vip.163.com
Yi-Fan Guo
20193071@zcmu.edu.cn

Full list of author information is available at the end of the article

Trial registration This study was approved by the Beijing Friendship Hospital Ethics Board (ClinicalTrials.gov Identifier: NCTO5137470) and conducted in accordance with the Declaration of Helsinki ethical standards.

Keywords Basal ganglia, Chronic kidney disease, Cognitive impairment, Quantitative susceptibility mapping, Radiomics

Background

Chronic kidney disease (CKD) is a significant global public health problem, exhibiting a high incidence and prevalence worldwide, affecting over 10% of the general population, encompassing more than 800 million individuals [1]. Patients with CKD face a multitude of complications, including the anemia, cognitive impairment (CI), mineral and bone disorders, as well as significantly elevated overall and cardiovascular mortality rates [2]. It is worth noting that CI varies in incidence from 16 to 38%, depending on the stage of CKD [3]. Therefore, regular screening is necessary for the early identification of CI and to implement targeted interventions.

QSM is widely used to quantify the spatial distribution of brain susceptibility value, which is helpful for detecting and analyzing brain iron deposition [4, 5]. Our previous studies have demonstrated that alterations in the susceptibility value of specific brain regions, as detected by quantitative susceptibility mapping (QSM), are associated with the cognitive status of patients with CKD [6, 7]. This finding suggests that these susceptibility value changes could serve as a potential biomarker for diagnosing CKD-related CI. One of the primary reasons our previous research efforts were unable to develop a precise diagnostic tool for CKD-related CI based on QSM is that traditional methods for measuring susceptibility values fail to capture the heterogeneity of iron deposition.

Habitat analysis can divide the target area into subregions by identifying gray voxel with similar imaging characteristics, which has the potential to better distinguish the heterogeneity of the target area [8]. Combining radiomics based on habitat analysis with QSM allows for an in-depth investigation of the heterogeneity of susceptibility values in the basal ganglia. This approach facilitates the investigation of iron deposition heterogeneity associated with CI within the basal ganglia of CKD patients. In recent years, radiomics has been applied to magnetic resonance imaging [9] to analyze the heterogeneity of preselected brain regions for the study of CI-related diseases [10, 11]. However, no studies have employed habitat-based radiomics to analyze the heterogeneity of iron deposition related to CI within the basal ganglia of CKD patients.

The objective of this study was to combine QSM and habitat-based radiomics to construct models that can accurately diagnose the cognitive status of CKD patients. Furthermore, we utilized habitat-based radiomics to explore the deep underlying relationship between the heterogeneity of iron deposition in the basal ganglia and CKD-related CI.

Methods

Study participants

This study was approved by the Beijing Friendship Hospital Ethics Board (ClinicalTrials.gov Identifier: NCTO5137470) and conducted in accordance with the Declaration of Helsinki ethical standards. Consecutive patients attending the Nephrology Department of Beijing Friendship Hospital, Capital Medical University, were invited to participate. Written informed consent was obtained from all participants or their relatives or guardians. The inclusion criteria were: (I) right-handedness; (II) age > 18 years; and (III) a CKD diagnosis based on the National Kidney Foundation-Kidney Disease Outcomes Quality Initiative guidelines [12]. The exclusion criteria were: (I) central nervous system diseases, including cerebrovascular diseases, trauma, and tumors; (II) significant carotid artery stenosis and intracranial artery stenosis; (III) drug or alcohol abuse; (IV) vertigo or intolerance of magnetic resonance imaging (MRI) scanning; and (V) psychiatric disorders (Fig. 1).

Clinical data, including blood biochemistry and cognitive assessment, were acquired within 24 h after MRI scanning. The Montreal Cognitive Assessment [13] test was used to evaluate the cognitive level of CKD patients. CKD patients with a threshold score of 26 or above were considered to have normal cognition, while those with scores below 26 were considered to have CI [14].

MRI acquisition and QSM reconstruction

The imaging was performed using a 3D multiple spoiled gradient echo sequence with flow compensation and multiple echo acquisitions. The parameters were set as follows: TR = 42.3 ms; TE = 3.3, 5.6, 8.0, 10.3, 12.7, 15.0, 17.4, 19.7 ms; flip angle = 15°; slice thickness = 1 mm; inter-slice gap = 0 mm; matrix = 256 × 256; FOV = 240 mm×240 mm. A total of 2240 axial slices were acquired. A monopolar readout gradient was used in the acquisition to minimize echo spacing and avoid phase-related artifacts inherent to bipolar readout.

The QSM images were reconstructed using the STI Suite (version 3.0; https://people.eecs.berkeley.edu/~chunlei.liu/software.html). Initially, phase images were unwrapped using the Laplacian method, which resulted in phase images containing a significant amount of background phase noise. Subsequently, background phase

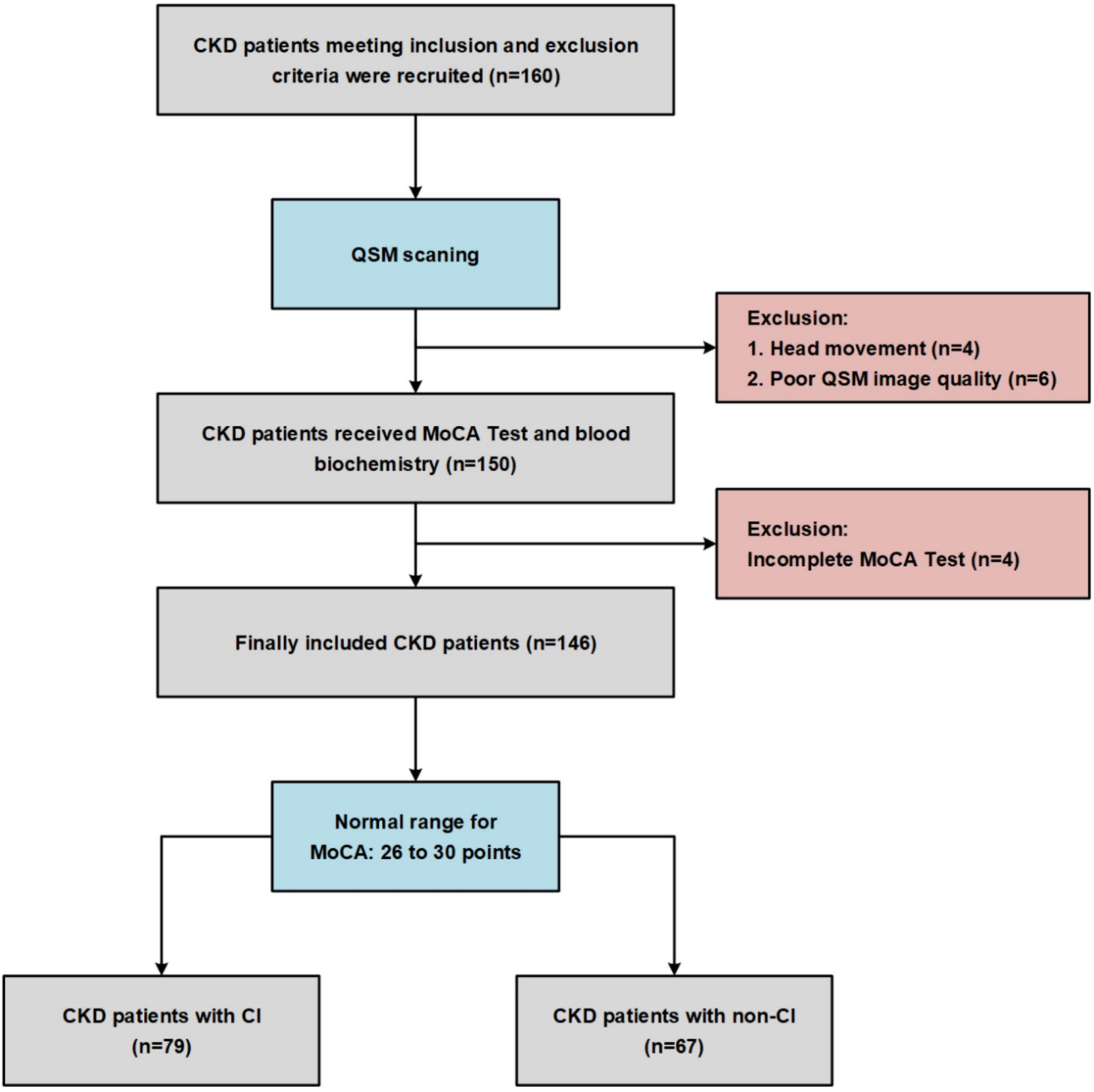

Fig. 1 Summary of patients with CI and non-CI recruitment and exclusions. CI, cognitive impairment; CKD, chronic kidney disease; MoCA, Montreal Cognitive Assessment; QSM, quantitative susceptibility mapping

noise was eliminated using a variable spherical kernel size approach for complex harmonic artifact reduction, where the radius of the spherical kernel increased from 1 mm at the brain's edge to 25 mm towards the center of the brain. Finally, an improved least squares orthogonal decomposition method was utilized to extract the QSM images from the phase images with background noise removed [15, 16]. The average magnetic susceptibility of cerebrospinal fluid within the lateral ventricle was used as the zero reference region, thereby ensuring a standardized baseline for magnetic susceptibility quantification.

Basal ganglia segmentation and susceptibility measurement

The segmentation of QSM images in this study was accomplished using ITK-SNAP (version 4.0.0; http://www.itksnap.org/pmwiki/pmwiki.php) [17]. The region of interest (ROI) for basal ganglia encompassed the globus pallidus, putamen, and caudate nucleus. Manual segmentation along the edges of the basal ganglia was performed on QSM images. All ROIs were delineated by a radiologist (Y Qi) with over 10 years of experience in neuroimaging diagnosis. Subsequently, the ROIs were reviewed

and refined by another radiologist (YF Guo) with more than 10 years of experience in neuroimaging diagnosis. According to our previous research, the mean susceptibility values of each nucleus (in units of parts per million [PPM]) were calculated by averaging the values across all consecutive slices [18].

Habitat area generation

In this study, ROIs were segmented into multiple subregions (i.e., habitats) based on voxel susceptibility values and radiomic features. Radiomic features included three first-order statistical features and eight Gray-level Co-occurrence Matrix (GLCM) features (Table 1) [19]. The voxel-level radiomic feature values were obtained by extracting and analyzing features from the image region surrounding each voxel. The K-means clustering algorithm was employed to classify voxels into different habitats based on their susceptibility values and feature values. To identify the optimal number of habitats, we assessed the clustering results using the average Calinski-Harabasz score and the Silhouette coefficient for each k value, based on 100 replicates. The study explored habitat numbers ranging from 2 to 5. Furthermore, habitat-based models were developed for each number of habitats to compare their effectiveness in predicting CKD-related CI.

Radiomic features extraction

Based on QSM, a total of 1197 features were extracted each segmented habitat area and the entire ROI. Thus, 1197 features were extracted for each of these 12 categories. The feature set of 1197 includes the following types: 234 first-order statistical features, 286 GLCM features, 182 Gy Level Dependence Matrix (GLDM) features, 208 Gy Level Run Length Matrix (GLRLM) features, 208 Gy Level Size Zone Matrix (GLSZM) features, 65 Neighboring Gray Tone Difference Matrix (NGTDM) features, and 14 shape features.

Features selection and habitat-based models construction

When constructing the habitat-based model, in addition to features extracted from individual habitats, features extracted from the entire basal ganglia were also used for feature selection and modeling. This study also built a predictive model based on the entire basal ganglia. Data preprocessing included unifying units, imputing missing values, and processing outliers. Pearson correlation coefficients were calculated to eliminate features with high correlations (>0.90). The minimum redundancy maximum relevance method was employed to screen the top 20 features with the strongest correlation to the categorical variables, aiding in identifying the most critical features. The random forest algorithm was used to construct prediction models. By comparing the area under the curve (AUC) values of all models on the test set, the best-performing model was selected for constructing the combined model. Figure 2 depicts a flowchart illustrating the process of constructing habitat-based models in this study.

Clinical and combined models construction

The predicted values output by the habitat-based model with the best predictive performance were used as a variable, along with clinical features, to construct the combined model. In this study, we employed multivariable logistic regression to develop clinical models and

Table 1 Habitat features and descriptions

Habitat feature	Description
First-order statistical feature	
Original_firstorder_Entropy	Entropy, reflecting the randomness and complexity of the image grayscale distribution.
Original_firstorder_MeanAbsoluteDeviation	Mean absolute deviation, indicating the average deviation of image grayscale values from the mean grayscale value.
Original_firstorder_Median	Median, representing the median grayscale value of the image.
GLCM feature	
Original_glcm_DifferenceAverage	Difference average of grayscale, describing the average difference in grayscale between pixel pairs.
Original_glcm_DifferenceEntropy	Difference entropy of grayscale, measuring the entropy of grayscale differences between pixel pairs.
Original_glcm_DifferenceVariance	Difference variance of grayscale, reflecting the variability of grayscale differences between pixel pairs.
Original_glcm_Imc1	Information measure of correlation 1, quantifying the irregularity of texture in the image.
Original_glcm_Imc2	Information measure of correlation 2, an alternative method for measuring texture irregularity.
Original_glcm_InverseVariance	Inverse variance, used to measure the uniformity of image texture.
Original_glcm_JointEnergy	Joint energy, reflecting the uniformity and repetitiveness of texture.
Original_glcm_JointEntropy	Joint entropy, measuring the irregularity and complexity of image texture.
Original_glcm_SumEntropy	Sum entropy, the total entropy sum of all elements in the joint matrix.

GLCM: Gray Level Co-occurrence Matrix

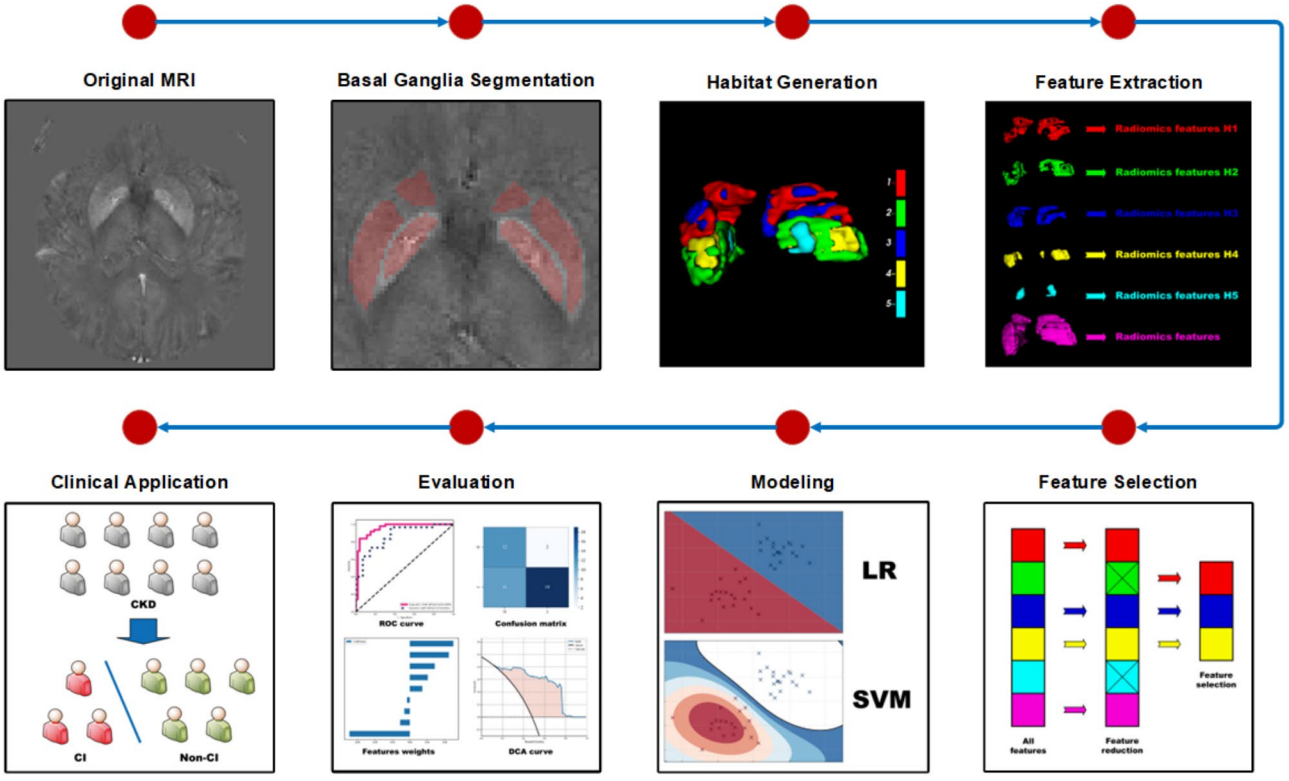

Fig. 2 This workflow provides a comprehensive approach to utilizing QSM and habitat-based radiomics for identifying CKD-related CI. First, obtain QSM images of CKD patients. Next, manually segment the basal ganglia on the QSM images and generate multiple habitats. Then, extract radiomic features from these segments. Subsequently, perform feature selection to construct models and evaluate their diagnostic performance. The ultimate goal is to develop a model that can accurately identify CKD-related CI for clinical application. CI, cognitive impairment; CKD, chronic kidney disease; QSM, quantitative susceptibility mapping

combined models. We utilized a stepwise regression method based on the Akaike information criterion, integrating both forward selection and backward elimination strategies. These models were evaluated using decision curve analysis (DCA) in practical clinical applications.

Statistical analyses

All statistical analyses were performed using R software (version 3.6.0; R Foundation). The Shapiro-Wilk test was employed to evaluate the normality of the distribution of patient demographic data. For continuous variables, normally distributed data were analyzed using the independent t-test, while non-normally distributed data were assessed using the Mann-Whitney U test. Categorical variables were examined using either the chi-square test or Fisher's exact test, depending on the suitability for the data. When comparing susceptibility values between CI and the non-CI groups, age, gender, and CKD stage were used as covariates. The predictive performance of all models was evaluated using receiver operating characteristic (ROC) analysis. The Hosmer-Lemeshow test was utilized to assess the fitting of the random forest model to determine potential overfitting. SHapley Additive exPlanations (SHAP) analysis was conducted to interpret the importance and contribution of individual radiomic features in predicting CKD-related CI. A two-tailed *P* value of less than 0.05 was considered statistically significant.

Results

Patient characteristics

This study included a total of 146 patients (mean age, 51 ± 13 years; 92 male) with CKD, with a MoCA score of 24.6 ± 3.6. Among these patients, 79 scored below the CI threshold of 26. Significant statistical differences were observed between the CI and non-CI groups in terms of age, serum urea, CKD stage, parathyroid hormone (PTH), and serum creatinine (all $p < 0.05$). However, there were no significant differences between the CI and non-CI groups regarding hemoglobin, serum phosphorus, serum iron, serum calcium, serum albumin, gender, total iron-binding capacity (TIBC), ferritin, and uric acid (all $p > 0.05$). In the training set, which included 102 patients, 49 were identified as having CI, while in the test set, which included 44 patients, 25 were identified as having CI. The distribution of clinical characteristics in the training and test sets, along with the *P* values between the CI and non-CI groups, are detailed in Table 2.

Table 2 Clinical characteristics of training and test sets

Characteristic	Training set (*n* = 102)	Test set (*n* = 44)	*P* value
Age, yr [a]	50.9 ± 12.5	52.2 ± 14.4	< 0.001 [b]
Gender			0.659 [c]
Male	62 (58.8%)	30 (68.2%)	
Female	40 (39.2%)	14 (31.8%)	
CKD stage			0.013 [c]
Stage 1	22 (21.6%)	3 (6.8%)	
Stage 2	15 (14.7%)	7 (15.9%)	
Stage 3	15 (14.7%)	7 (15.9%)	
Stage 4	3 (2.9%)	0 (0%)	
Stage 5	47 (46.1%)	27 (61.4%)	
Ferritin [a]	92.2 ± 81.8	155.7 ± 208.1	0.902 [b]
Hemoglobin [a]	114.1 ± 24.6	108.8 ± 26.3	0.064 [d]
PTH [a]	146.1 ± 187.7	196.4 ± 242.7	0.034 [b]
Serum albumin [a]	34.3 ± 6.2	33.6 ± 7.2	0.350 [b]
Serum calcium [a]	2.2 ± 0.2	2.1 ± 0.3	0.168 [b]
Serum creatinine [a]	414.9 ± 376.8	500.5 ± 363.8	0.018 [b]
Serum phosphorus [a]	1.6 ± 0.6	6.2 ± 29.1	0.106 [b]
Serum urea [a]	17.7 ± 13.1	20.6 ± 12.3	0.008 [b]
Serum iron [a]	12.7 ± 6.5	13.2 ± 8.0	0.164 [b]
TIBC [a]	45.7 ± 9.6	44.9 ± 11.8	0.686 [d]
Uric acid [a]	419.1 ± 116.4	435.9 ± 110.2	0.948 [b]

Unless otherwise noted, data present the numbers of patients, with percentages in parentheses. CKD, chronic kidney disease; PTH, parathyroid hormone; TIBC: total iron-binding capacity

[a] Data are presented as means ± SDs

[b] Mann-Whitney U test

[c] Chi-square test

[d] Independent t-test

Prediction performance of susceptibility value

After adjusting for age, gender, and CKD stage, no statistically significant differences were found in the susceptibility value of all basal ganglia nuclei between the CI and non-CI groups, as determined by the Mann-Whitney U test (all $p > 0.05$). The predictive ability of susceptibility value in various basal ganglia nuclei for CKD-related CI is limited. In the training and testing sets, the AUCs for the susceptibility value of the basal ganglia nuclei ranged from 0.445 to 0.594 and 0.429 to 0.573, respectively (Table 3).

Prediction performance of habitat-based models

The optimal number of habitats was determined to be two based on the Calinski-Harabasz score and Silhouette coefficient (Fig. 3A). When the number of habitats was set to two, the habitat distribution in the basal ganglia was generally symmetrical on both sides and did not correspond to the anatomical structure of the basal ganglia regions (Fig. 3B).

SHAP analysis revealed that radiomic features extracted from the entire basal ganglia (∑mean|SHAP value| = 0.247) and habitat 2 (∑mean|SHAP value| = 0.183) significantly contributed to the model for predicting CKD-related CI. Among the 19 features used to construct the two habitats-based model, only two radiomic features were extracted from habitat 1, and their overall contribution (∑mean|SHAP value| = 0.066) was lower compared to the other two feature sets. However, the individual features from habitat 1 had relatively high contributions to the prediction of the model (Fig. 4). Based on differences in feature composition, habitat 2 was characterized by higher susceptibility values and a greater proportion of first-order intensity features and high-frequency wavelet-based texture descriptors, indicating more pronounced radiomic variability. In contrast, habitat 1 consisted of lower susceptibility values and a higher proportion of lower-frequency texture and statistical homogeneity features, suggesting more stable radiomic patterns. Therefore, habitat 2 in the basal ganglia of CKD patients was highly associated with CI, whereas habitat 1 exhibited the opposite trend.

The two habitats-based model also demonstrated superior predictive ability for CKD-related CI compared to other habitat-based models (Table 3). The AUCs of the two habitats-based model in the training and test sets were 0.957 (95% CI: 0.918–0.997) and 0.926 (95% CI: 0.843-1.000), respectively (Fig. 5A and B).

Prediction performance of clinical and combined models

Through multivariate logistic regression analysis, age, gender, CKD stage, serum urea, serum creatinine, uric acid, serum albumin, serum calcium, serum phosphorus, PTH, ferritin, serum iron, TIBC, and hemoglobin were included in the clinical model. The clinical model achieved AUCs of 0.831 (95% CI: 0.747–0.915) in the training set and 0.792 (95% CI: 0.648–0.935) in the test set (Table 3). Subsequently, these clinical characteristics were combined with the predicted values from the two habitats-based model to develop the combined model. This combined model achieved AUCs of 0.971 (95% CI: 0.946–0.996) in the training set and 0.910 (95% CI: 0.829–0.992) in the test set (Table 3; Fig. 5A and B).

Comparison of prediction models

In the test set, the two habitats-based model achieved an AUC of 0.926, which was higher than the susceptibility value of the basal ganglia and its nuclei (AUC: 0.429–0.573), other habitat-based models (AUC: 0.622–0.802), the clinical model (AUC: 0.792), and the combined model (AUC: 0.910). The DCA results indicated that the clinical utility of the two habitats-based model was higher than that of the clinical model and combined model (Fig. 5C).

Discussion

Our previous studies have proposed that susceptibility value serves as a biomarker for diagnosing cognitive status in patients with CKD [7]. This study used a

Table 3 Predictive performance of various models on train and test sets

Models	Sets	AUC	95 CI%	ACC	SEN	SPE	NPV	PPV
CNL-L	Training	0.51	0.40–0.63	0.49	0.47	0.51	0.45	0.53
	Test	0.46	0.29–0.64	0.52	0.46	0.60	0.48	0.58
CNL-R	Training	0.58	0.47–0.69	0.58	0.55	0.62	0.54	0.63
	Test	0.43	0.25–0.61	0.41	0.38	0.45	0.38	0.45
PUT-L	Training	0.55	0.43–0.66	0.47	0.42	0.53	0.44	0.51
	Test	0.57	0.40–0.75	0.55	0.54	0.55	0.50	0.59
PUT-R	Training	0.59	0.48–0.71	0.57	0.53	0.62	0.53	0.62
	Test	0.57	0.40–0.75	0.57	0.58	0.55	0.52	0.61
GPL-L	Training	0.44	0.33–0.56	0.47	0.47	0.47	0.43	0.51
	Test	0.49	0.31–0.67	0.52	0.42	0.65	0.48	0.59
GPL-R	Train	0.54	0.42–0.65	0.50	0.51	0.49	0.46	0.54
	Test	0.51	0.33–0.69	0.52	0.46	0.60	0.48	0.58
Basal ganglia	Training	0.93	0.87–0.98	0.89	0.87	0.92	0.86	0.92
	Test	0.77	0.63–0.91	0.71	0.67	0.75	0.65	0.76
Two habitats	Training	0.96	0.92-1.00	0.93	0.98	0.87	0.98	0.90
	Test	0.93	0.84-1.00	0.86	0.96	0.75	0.94	0.82
Three habitats	Training	0.94	0.90–0.99	0.88	0.91	0.85	0.89	0.88
	Test	0.69	0.53–0.85	0.66	0.58	0.75	0.60	0.74
Four habitats	Training	0.91	0.85–0.97	0.87	0.87	0.87	0.85	0.89
	Test	0.62	0.45–0.79	0.57	0.34	0.80	0.52	0.69
Five habitats	Training	0.98	0.86-1.00	0.92	0.93	0.92	0.92	0.93
	Test	0.80	0.65–0.95	0.77	0.75	0.80	0.73	0.82
Clinical	Training	0.83	0.75–0.91	0.80	0.83	0.78	0.81	0.80
	Test	0.79	0.65–0.93	0.75	0.70	0.79	0.76	0.74
Combined	Training	0.97	0.95-1.00	0.87	0.87	0.88	0.86	0.88
	Test	0.91	0.83–0.99	0.80	0.90	0.71	0.89	0.72

AUC: Area Under the Curve; ACC: Accuracy; CNL-L: Left Caudate Nucleus; CNL-R: Right Caudate Nucleus; CI: Confidence Interval; GPL-L: Left Globus Pallidus; GPL-R: Right Globus Pallidus; NPV: Negative Predictive Value; PPV: Positive Predictive Value; PUT-L: Left Putamen; PUT-R: Right Putamen; SEN: Sensitivity; SPE: Specificity

habitat-based quantitative method to analyze basal ganglia susceptibility value and successfully constructed a random forest model for the precise diagnosis of CKD-related CI.

Cognitive changes can occur in the early stages of CKD when GFR drops to < 60 ml/min/1.73 m^2 or even earlier [20, 21]. However, in end-stage renal disease, there is no significant correlation between subjective cognitive symptoms and objective CI [3, 20, 22]. Therefore, regular screening is crucial for the early identification of CI and timely intervention. In clinical practice, the Mini-Mental State Examination (MMSE) and the MoCA are primary screening tools for CI [13]. However, repeated use of these assessments can lead to practice effects, where patients improve scores due to familiarity with the test, thus reducing their sensitivity in detecting true cognitive decline. Furthermore, a previous study reported that although healthcare providers and haemodialysis technicians spend an average of 47 min with each patient during each treatment session two to three times a week, mental disorders in these patients are often under-recognized [23]. There is an urgent need for an objective method that can independently identify CKD-related CI. The two habitats-based model developed in this study is a potential screening tool for identifying CKD-related CI. This model demonstrated a higher clinical net benefit compared to both the clinical model and the combined model. The two habitats-based model does not rely on clinical characteristics and can accurately identify CI at various stages of CKD, making it suitable for widespread and repeated use in CKD populations. Given the limitations in sensitivity of current screening tools (such as MMSE and MoCA), the two habitats-based model proposed in this study offers a potential new approach for the early and accurate identification of CKD-related CI in the future.

This study combines QSM and habitat analysis techniques to explore the heterogeneity of iron deposition in patients with CKD. Disruption of iron balance, caused by factors such as inflammation [24], aging [25], and oxidative stress [26], plays a critical role in iron metabolism and can result in cellular damage and neurological diseases. CKD is marked by oxidative stress and inflammation, both of which contribute to CKD progression and can lead to cardiovascular disease and other complications [27, 28]. Iron deposition heterogeneity is influenced by multiple mechanisms. Using the habitat analysis method, the heterogeneity of iron deposition in the basal

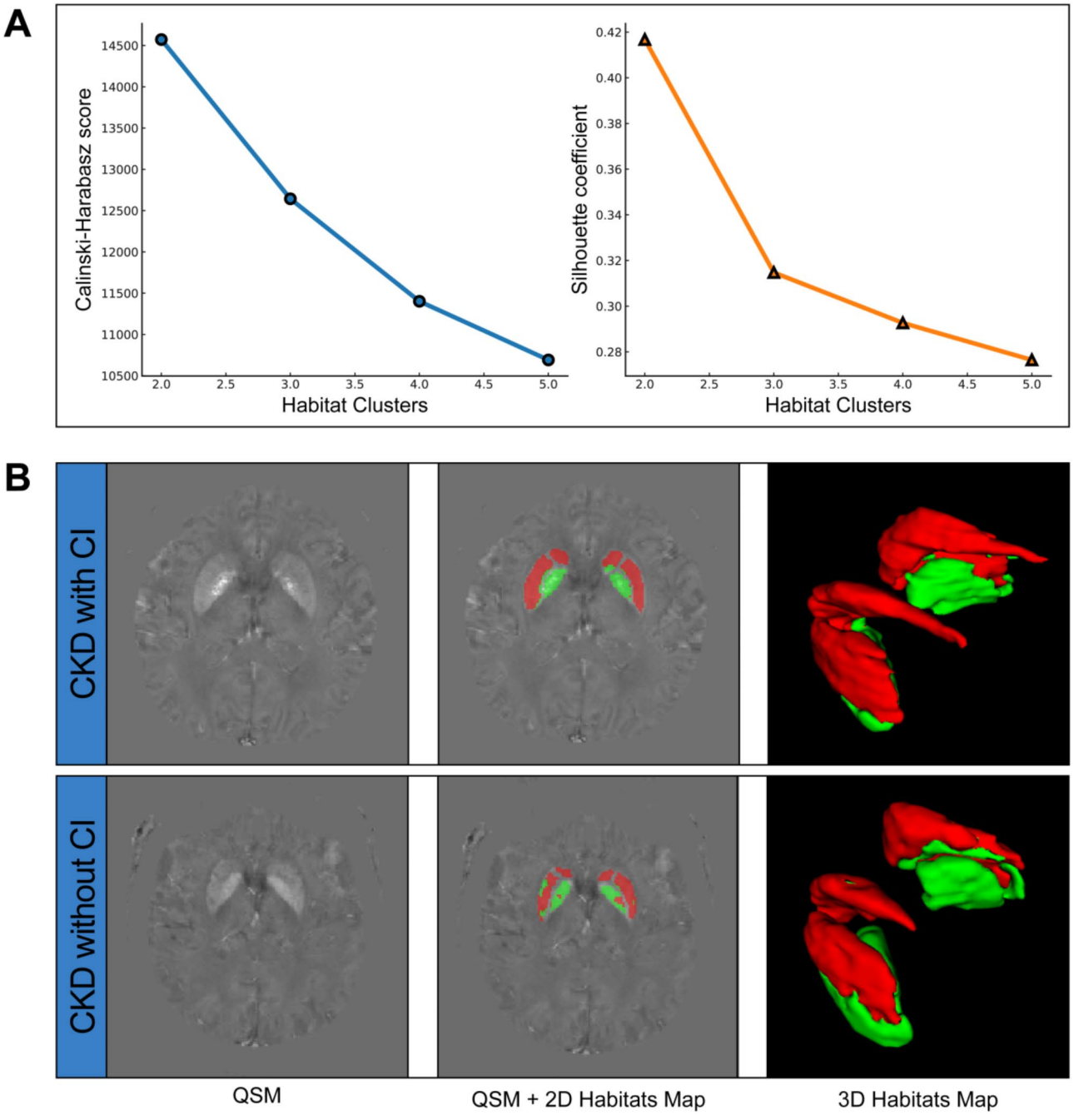

Fig. 3 (**A**) Calinski-Harabasz score and Silhouette coefficient plots used to determine the optimal number of habitats. (**B**) Two-habitat maps of CKD patients with and without CI, respectively. CI, cognitive impairment; CKD, chronic kidney disease; QSM, quantitative susceptibility mapping

ganglia can be interpreted from multiple dimensions, making the features of iron deposition heterogeneity under a single mechanism more apparent. The two-habitat maps revealed that iron deposition in the basal ganglia under the influence of CKD primarily follows two distribution patterns, which are associated with the cognitive status of CKD patients. Notably, the habitat distribution in the basal ganglia did not closely match the anatomical locations of the globus pallidus, lentiform nucleus, and putamen. Previous clinical imaging studies on CKD typically analyze individual nuclear masses as independent entities [29, 30]. However, these findings provide a novel perspective for research on CKD-related CI.

The basal ganglia, as a complex brain region, may exhibit different distributions and concentrations of iron deposition in its various subregions. This heterogeneity likely reflects its diverse roles in cognitive function [31, 32]. Simple measurements of average susceptibility

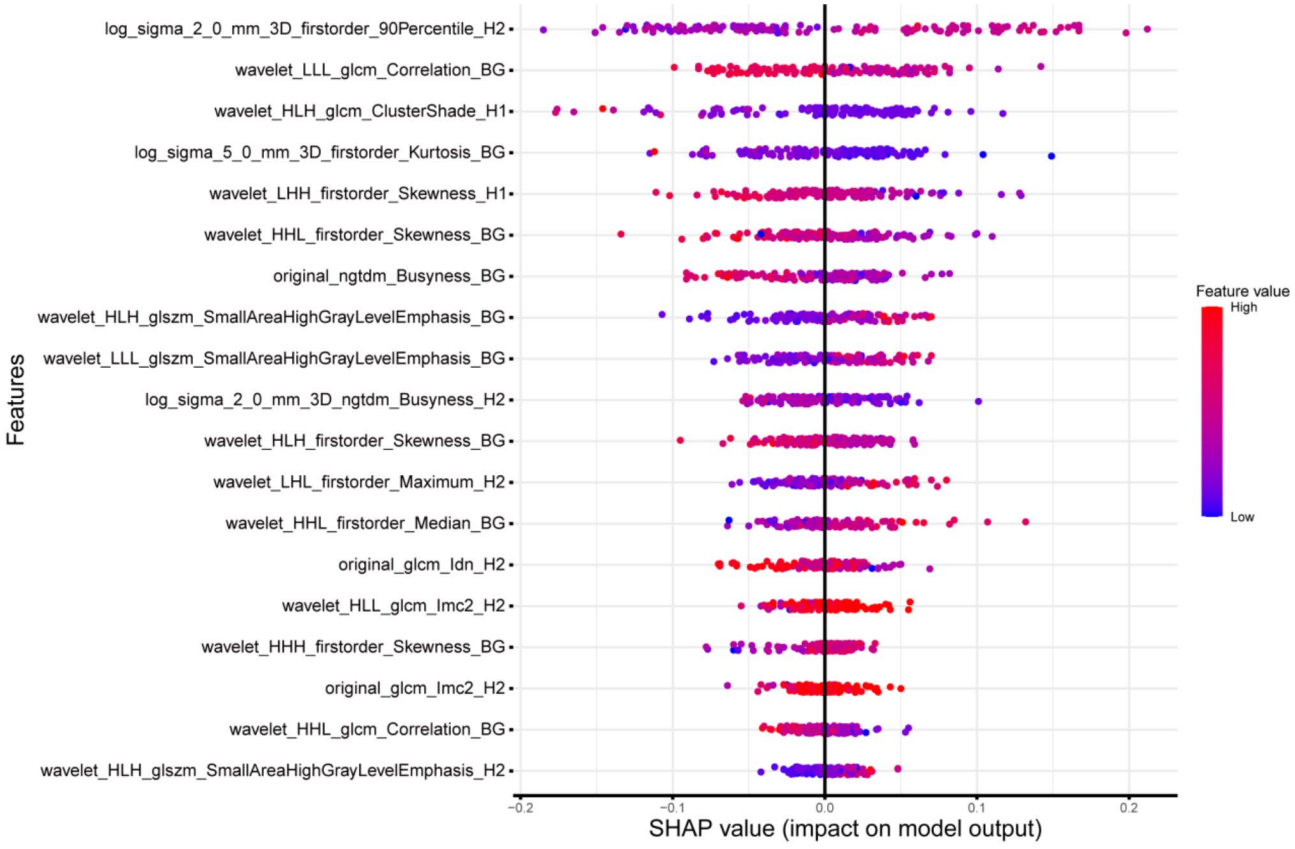

Fig. 4 Beeswarm plot of the SHAP analysis of the two habitats-based model. SHAP, SHapley Additive exPlanations

values in the basal ganglia region cannot capture this heterogeneity, and the loss of this crucial information is the primary reason why the susceptibility values of the basal ganglia region perform poorly in diagnosing CKD-related CI. This study found that features extracted from the entire basal ganglia had a significant impact on predicting CKD-related CI in the two habitats-based model, which supports our viewpoint. Radiomic features from habitat 2 also substantially contributed to the model's prediction of CKD-related CI. We hypothesize that habitat 2 might be a susceptible area to CKD's effects on iron deposition in the basal ganglia, containing a wealth of CI-related quantitative information. Although the overall contribution of habitat 1 is lower, individual features within this region have high contribution values. Habitat 1 might be a resistant area to CKD's effects on iron deposition in the basal ganglia, containing less CI-related quantitative information. However, once this area is affected, the radiomic features reflecting the heterogeneity of iron deposition highly specifically indicate CI. The heterogeneity of iron deposition might be the key to solving the diagnosis and treatment of CKD-related CI, but more research is needed to explore and validate this hypothesis.

This study has certain limitations. The sample size is relatively small. Therefore, we selected the random forest algorithm to construct habitat-based models due to its robustness with small datasets, its effectiveness in avoiding overfitting through ensemble learning, and its capability to handle high-dimensional data. Larger prospective datasets are needed to further validate and improve the predictive performance of our model. Additionally, this study proposes that CKD may influence the distribution of iron deposition in the basal ganglia through two distinct patterns based on the results of habitat analysis. This finding and the associated hypotheses require further validation through histopathological studies.

Conclusions

This study applied a habitat-based quantitative analysis technique to the basal ganglia in QSM and successfully develop a two habitats-based model capable of accurately identifying CKD-related CI. This study presents an objective method independent of clinical information, with the potential to become a tool for routine screening of CI in CKD. Additionally, this study suggests that the effects of CKD on the basal ganglia are characterized by a dual-mode distribution of iron deposition, providing a potential research direction for the study of CKD-related CI in the basal ganglia.

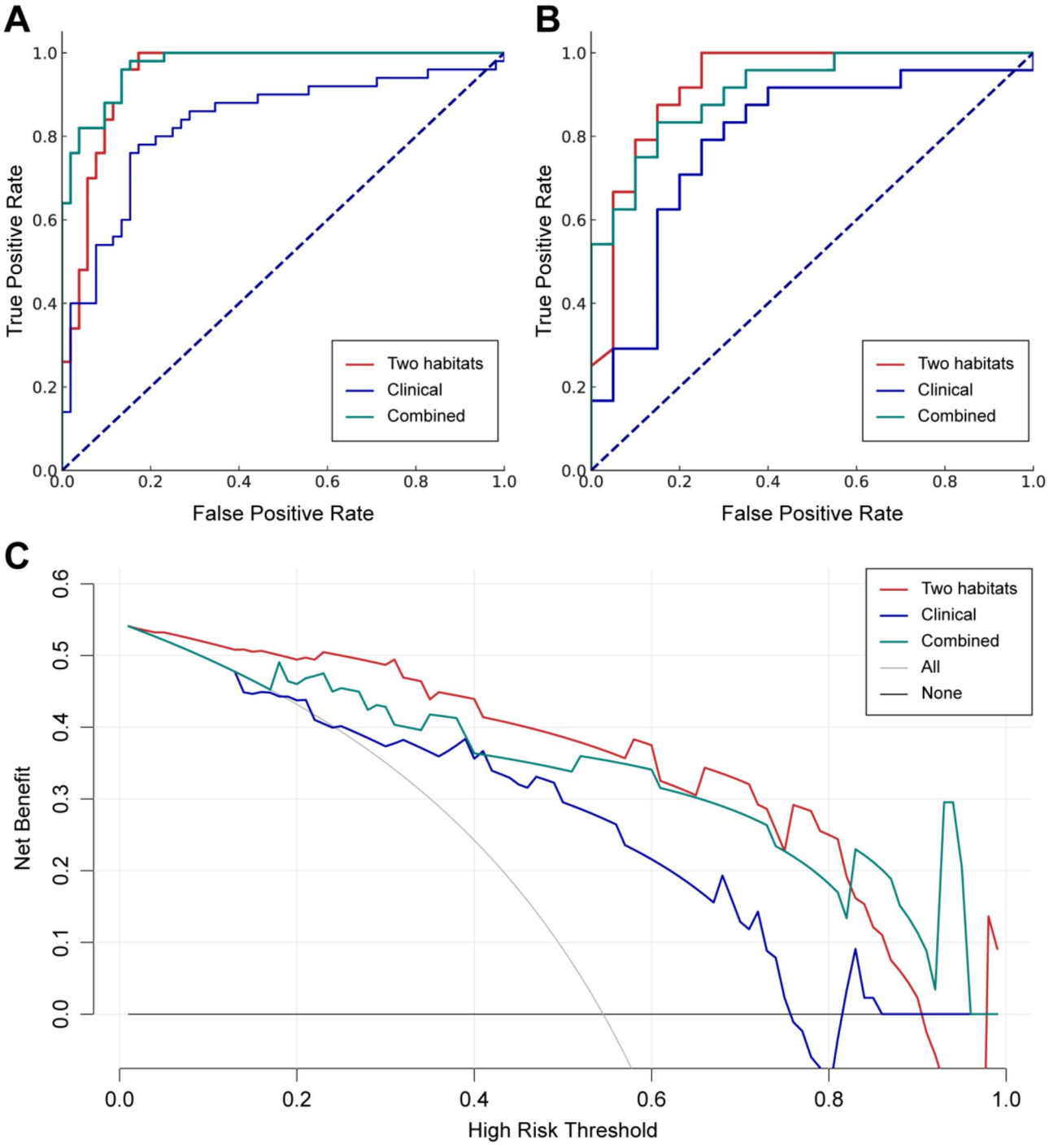

Fig. 5 ROC curves of various CKD-related CI prediction models in the training set (**A**) and test set (**B**). The DCA of the Two habitats-based model, clinical model, and combined model in the test set (**C**). CI, cognitive impairment; CKD, chronic kidney disease; DCA, decision curve analysis

Abbreviations

CI	Cognitive Impairment
CKD	Chronic Kidney Disease
MRI	Magnetic Resonance Imaging
NGTDM	Neighboring Gray Tone Difference Matrix
GLCM	Gray-level Co-occurrence Matrix
GLDM	Gray Level Dependence Matrix
GLRLM	Gray Level Run Length Matrix
GLSZM	Gray Level Size Zone Matrix
QSM	Quantitative Susceptibility Mapping
SHAP	SHapley Additive exPlanations

Acknowledgements
Not applicable.

Author contributions
Z.C.W. conceptualized the study. M.L., L.S., W.B.Y., X.L., and X.Y.B. curated the data. Y.Q., H.N.Z., Y.Z.L., S.Q.C., and Y.W. conducted formal analysis. Y.F.G. and

H.W. drafted the original manuscript. M.S.X., Z.C.W., and Z.H.Y. reviewed and edited the manuscript.

Funding
This study has received funding by the National Natural Science Foundation of China (82202099 and 52227814), Beijing Municipal Administration of Hospitals Clinical Medicine Development of Special Funding Support (contract grant numbers: ZYLX201824 and ZYLX202101), Beijing Municipal Administration of Hospital's Mission Plan (contract grant number: SML20150101), Beijing Scholar 2015 (Zhenchang Wang), Beijing Friendship Hospital, Capital Medical University (contract grant number: seed project YYZZ202129, yyqcjh2023-7), and Training Fund for Open Projects at Clinical Institutes and Departments of Capital Medical University (CCMU2022ZKYXY011).

Data availability
The data that support the findings of this study are available from the Beijing Friendship Hospital but restrictions apply to the availability of these data, which were used under license for the current study, and so are not publicly available. Data are however available from the authors upon reasonable request and with permission of the Beijing Friendship Hospital.

Declarations

Ethics approval and consent to participate
This study was approved by the Beijing Friendship Hospital Ethics Board (ClinicalTrials.gov Identifier: NCTO5137470) and was conducted in accordance with the ethical standards of the Declaration of Helsinki. Written informed consent was obtained from all subjects (patients) prior to participation in the study.

Consent for publication
Not applicable.

Competing interests
The authors declare no competing interests.

Author details
[1]Department of Radiology, Beijing Friendship Hospital, Capital Medical University, No. 95 Yong An Road, Xicheng District, Beijing 100050, China
[2]Department of Radiology, The Affiliated Drum Tower Hospital of Nanjing University Medical School, Nanjing, Jiangsu, China
[3]Department of Nephrology, Beijing Friendship Hospital, Capital Medical University, Beijing, China
[4]Department of Radiology, The First Affiliated Hospital of Zhejiang Chinese Medical University (Zhejiang Provincial Hospital of Traditional Chinese Medicine), Hangzhou, Zhejiang, China
[5]The First School of Clinical Medicine, Zhejiang Chinese Medical University, Hangzhou, Zhejiang, China
[6]Center of Radiology, The Second Affiliated Hospital of Fujian Medical University, Quanzhou, Fujian, China
[7]School of Medical Imaging, Fujian Medical University, Fuzhou, Fujian, China

Received: 21 November 2024 / Accepted: 1 April 2025
Published online: 08 April 2025

References

1. Kovesdy CP. Epidemiology of chronic kidney disease: an update 2022. Kidney Int Supplements. 2022;12(1):7–11.
2. Kalantar-Zadeh K, Jafar TH, Nitsch D, Neuen BL, Perkovic V. Chronic kidney disease. Lancet. 2021;398(10302):786–802.
3. Kurella Tamura M, Yaffe K. Dementia and cognitive impairment in ESRD: diagnostic and therapeutic strategies. Kidney Int. 2011;79(1):14–22.
4. Haacke EM, Liu S, Buch S, Zheng W, Wu D, Ye Y. Quantitative susceptibility mapping: current status and future directions. Magn Reson Imaging. 2015;33(1):1–25.
5. Vinayagamani S, Sheelakumari R, Sabarish S, Senthilvelan S, Ros R, Thomas B, et al. Quantitative susceptibility mapping: Technical considerations and clinical applications in neuroimaging. J Magn Reson Imaging: JMRI. 2021;53(1):23–37.
6. Wang H, Liu X, Song L, Yang W, Li M, Chen Q, et al. Dysfunctional coupling of cerebral blood flow and susceptibility value in the bilateral hippocampus is associated with cognitive decline in nondialysis patients with CKD. J Am Soc Nephrology: JASN. 2023;34(9):1574–88.
7. Wang H, Song L, Li M, Yang Z, Wang ZC. Association between susceptibility value and cerebral blood flow in the bilateral putamen in patients undergoing hemodialysis. J Cereb Blood Flow Metabolism: Official J Int Soc Cereb Blood Flow Metabolism. 2023;43(3):433–45.
8. Shi Z, Huang X, Cheng Z, Xu Z, Lin H, Liu C, et al. MRI-based quantification of intratumoral heterogeneity for predicting treatment response to neoadjuvant chemotherapy in breast cancer. Radiology. 2023;308(1):e222830.
9. Hametner S, Endmayr V, Deistung A, Palmrich P, Prihoda M, Haimburger E, et al. The influence of brain iron and myelin on magnetic susceptibility and effective transverse relaxation - A biochemical and histological validation study. NeuroImage. 2018;179:117–33.
10. Park CJ, Eom J, Park KS, Park YW, Chung SJ, Kim YJ, et al. An interpretable multiparametric radiomics model of basal ganglia to predict dementia conversion in Parkinson's disease. NPJ Parkinson's Disease. 2023;9(1):127.
11. Tang L, Wu X, Liu H, Wu F, Song R, Zhang W, et al. Individualized prediction of early Alzheimer's disease based on magnetic resonance imaging radiomics, clinical, and laboratory examinations: A 60-month follow-up study. J Magn Reson Imaging: JMRI. 2021;54(5):1647–57.
12. Shlipak MG, Tummalapalli SL, Boulware LE, Grams ME, Ix JH, Jha V, et al. The case for early identification and intervention of chronic kidney disease: conclusions from a kidney disease: improving global outcomes (KDIGO) controversies conference. Kidney Int. 2021;99(1):34–47.
13. Pépin M, Ferreira AC, Arici M, Bachman M, Barbieri M, Bumblyte IA, et al. Cognitive disorders in patients with chronic kidney disease: specificities of clinical assessment. Nephrology, dialysis, transplantation: official publication of the European Dialysis and transplant association - European Renal Association. 2021;37(Suppl 2):ii23–32.
14. Nasreddine ZS, Phillips NA, Bédirian V, Charbonneau S, Whitehead V, Collin I, et al. The Montreal cognitive assessment, MoCA: a brief screening tool for mild cognitive impairment. J Am Geriatr Soc. 2005;53(4):695–9.
15. Li W, Wang N, Yu F, Han H, Cao W, Romero R, et al. A method for estimating and removing streaking artifacts in quantitative susceptibility mapping. NeuroImage. 2015;108:111–22.
16. Li W, Wu B, Liu C. Quantitative susceptibility mapping of human brain reflects spatial variation in tissue composition. NeuroImage. 2011;55(4):1645–56.
17. Yushkevich PA, Piven J, Hazlett HC, Smith RG, Ho S, Gee JC, et al. User-guided 3D active contour segmentation of anatomical structures: significantly improved efficiency and reliability. NeuroImage. 2006;31(3):1116–28.
18. Wang H, Han X, Jin M, Wang LY, Diao ZL, Guo W, et al. Different iron deposition patterns in hemodialysis patients with and without restless legs syndrome: a quantitative susceptibility mapping study. Sleep Med. 2020;69:34–40.
19. van Griethuysen JJM, Fedorov A, Parmar C, Hosny A, Aucoin N, Narayan V, et al. Computational radiomics system to decode the radiographic phenotype. Cancer Res. 2017;77(21):e104–7.
20. Berger I, Wu S, Masson P, Kelly PJ, Duthie FA, Whiteley W, et al. Cognition in chronic kidney disease: a systematic review and meta-analysis. BMC Med. 2016;14(1):206.
21. Murray AM. Cognitive impairment in the aging dialysis and chronic kidney disease populations: an occult burden. Adv Chronic Kidney Dis. 2008;15(2):123–32.
22. Leinau L, Murphy TE, Bradley E, Fried T. Relationship between conditions addressed by hemodialysis guidelines and non-ESRD-specific conditions affecting quality of life. Clin J Am Soc Nephrology: CJASN. 2009;4(3):572–8.
23. Sehgal AR, Grey SF, DeOreo PB, Whitehouse PJ. Prevalence, recognition, and implications of mental impairment among hemodialysis patients. Am J Kidney Diseases: Official J Natl Kidney Foundation. 1997;30(1):41–9.
24. Urrutia P, Aguirre P, Esparza A, Tapia V, Mena NP, Arredondo M, et al. Inflammation alters the expression of DMT1, FPN1 and hepcidin, and it causes iron accumulation in central nervous system cells. J Neurochem. 2013;126(4):541–9.
25. Loeffler DA, Connor JR, Juneau PL, Snyder BS, Kanaley L, DeMaggio AJ, et al. Transferrin and iron in normal, Alzheimer's disease, and Parkinson's disease brain regions. J Neurochem. 1995;65(2):710–24.

26. Masaldan S, Belaidi AA, Ayton S, Bush AI. Cellular Senescence and Iron Dyshomeostasis in Alzheimer's Disease. Pharmaceuticals (Basel Switzerland). 2019;12(2).
27. Viggiano D, Wagner CA, Martino G, Nedergaard M, Zoccali C, Unwin R, et al. Mechanisms of cognitive dysfunction in CKD. Nat Rev Nephrol. 2020;16(8):452–69.
28. Kishi S, Nagasu H, Kidokoro K, Kashihara N. Oxidative stress and the role of redox signalling in chronic kidney disease. Nat Rev Nephrol. 2024;20(2):101–19.
29. Hamed SA. Neurologic conditions and disorders of uremic syndrome of chronic kidney disease: presentations, causes, and treatment strategies. Expert Rev Clin Pharmacol. 2019;12(1):61–90.
30. Kang JJ, Chen Y, Xu GD, Bao SL, Wang J, Ge M, et al. Combining quantitative susceptibility mapping to radiomics in diagnosing Parkinson's disease and assessing cognitive impairment. Eur Radiol. 2022;32(10):6992–7003.
31. Rouault TA. Iron metabolism in the CNS: implications for neurodegenerative diseases. Nat Rev Neurosci. 2013;14(8):551–64.
32. Kruer MC, Boddaert N, Schneider SA, Houlden H, Bhatia KP, Gregory A, et al. Neuroimaging features of neurodegeneration with brain iron accumulation. AJNR Am J Neuroradiol. 2012;33(3):407–14.

Publisher's note